Glasslike excitations in chemically disordered crystals: Alkali-earth lanthanum fluoride mixed crystals

Karen A. Topp,* EunJoo Thompson, and R. O. Pohl
Laboratory of Atomic and Solid State Physics, Cornell University, Ithaca, New York 14853
(Received 2 February 1999)

Through measurements of internal friction and speed of sound at low temperatures we have followed the evolution of glasslike low-energy excitations in chemically disordered crystalline CaF_2 and SrF_2 containing increasing concentrations of LaF_3. Although small concentrations do exhibit relaxational processes at low temperatures, low-energy excitations that can be well described with the tunneling model are observed only when the LaF_3 concentration exceeds approximately 20 mol %. This result is shown to agree with the earlier results on BaF_2 containing LaF_3. In the mixed host $(BaF_2)_{0.5}(SrF_2)_{0.5}$, on the other hand, even small LaF_3 concentrations lead to excitations that are well described with the tunneling model. These results confirm the earlier findings by Watson [Phys. Rev. Lett. **75**, 1965 (1995)] that random stresses are essential for the creation of glasslike excitation in solids. [S0163-1829(99)10425-9]

I. INTRODUCTION

The lattice vibrations of perfect crystals, described as plane waves, can be altered by chemical imperfections. The resulting impurity modes can affect the thermal, elastic, and dielectric properties of the solid. As an example, we mention the quasirotational excitations of molecular ions in substitutional sites of alkali halide lattices, whose lowest motional states are described as tunneling states.[2] In amorphous solids, however, localized excitations dominate the vibrational spectra at low energies, and these determine the low temperature macroscopic properties regardless of their chemical composition or mode of preparation.[3] The excitations are described with the tunneling model,[4,5] in which atoms or groups of atoms are assumed to perform tunneling motions between energetically nearly equivalent positions. This model has two parameters, the spectral energy density of the tunneling systems, $\overline{P}$, which is nearly constant, and their coupling energies to the lattice, $\gamma_{l,t}$. These parameters are connected by a quantity C which is called the tunneling strength. The physical nature of these tunneling states is still unknown, and is the object of the present investigation. One of the difficulties in determining the tunneling entity is that the properties of amorphous solids are nearly independent of the chemical composition of the amorphous solids.[6] In fact, the most widely tested quantity, C, was compared for over 20 amorphous solids and found to lie in the range of 10^{-4} and 10^{-3}, often called the ''glassy range.''[7] (Recently, values of C have been determined for amorphous silicon and germanium and found to be somewhat below this range by a factor of roughly 3.[8])

The origin of these low-energy, localized excitations became more puzzling when it was discovered that very similar excitations were also observed through thermal and elastic measurements in a number of chemically disordered crystalline solids. We mention a few examples: the mixed crystal $(KBr)_{0.75}(KCN)_{0.25}$, in the orientational glass state;[9] the superconducting alloys $Ti_{0.63}Nb_{0.37}$ and $Ti_{0.67}V_{0.33}$ that contain both the omega and beta crystallographic phase;[10] ZrO_2:Y_2O_3 stabilized in the cubic phase;[11] the nearly stoichiometric boride YB_{63}, in which the Y ions randomly occupy one half of the lattice sites available to them;[12] the so-called dirty ferroelectrics, in which the chemical disorder leads to a broadening of the ferroelectric phase transition;[13,14] and finally, certain feldspars, in which alkali and alkali-earth ions are randomly distributed over interstitial sites.[15] We refer to a recent review of elastic and thermal-conductivity measurements on several of these solids that can be well described with the tunneling model, and whose tunneling strength C lies within the glassy range.[16]

The similarity of the low-energy excitations—called ''glasslike'' excitations[17]—in these chemically disordered crystalline solids to those seen in amorphous solids can be taken as evidence that they are identical to the tunneling states in amorphous solids. One would then conclude that the amorphous structure itself plays only a secondary role in their origin. Recently, this conclusion was strengthened by the observation that in hydrogenated a-Si prepared by hot-wire chemical-vapor deposition, the tunneling strength C is smaller than the glassy range by over a factor of 100 with a value as small as 5×10^{-7}.[18] This demonstrated unambiguously that the amorphous structure itself is not the cause for these low-energy excitations. Further persuasive evidence of their identical nature in both the crystalline and the amorphous phases has recently been obtained in crystalline silicon that had been disordered by ion implantation using both Si^+ and B^+ ions.[19] In both cases, using both internal friction and thermal conductivity measurements, low-energy excitations were found to evolve with increasing dose. They could be described with the tunneling model, with a tunneling strength C saturating at 2.1×10^{-5} for large doses, that is equal, within a factor of 2, to that of a-Si produced by sputtering.[8] Three important conclusions could be drawn from these results: (i) The evolution of these states was entirely unaffected by whether the silicon amorphized at high doses, as it does for Si^+ implantation, or whether it stayed a disordered crystalline, as it does for B^+ implantation. This identical behavior showed that the defects causing the low-energy excita-

tions in the disordered crystal (which are yet to be identified), somehow persist in the amorphous phase. (ii) The saturated level of the tunneling strength C remained unchanged over two orders of magnitude in dose. A hundredfold increase means a large increase in radiation damage,[20,21] and yet the tunneling strength was found to be unaffected. This observation demonstrated that the tunneling strength C in the glassy range somehow represents an upper limit, and whatever the limiting physical mechanism, it persists into the amorphous phase. (iii) Implantation leads to the formation of defects, with divacancies and di-interstitials being the smallest ones that are stable at room temperature.[20] Hence, the most plausible explanation is that the low-energy excitations are connected with these defects or some aggregates that have low-energy motional states. These defects cause random stresses in the lattice, which may lead to a splitting of the vibrational ground states of the defects, and thus lead to the tunneling states. Experimental evidence for the importance of random stresses is based on the recent observation of the formation of a uniform spectral density $\overline{P}$ of tunneling states from the tunneling states of isolated CN^- ions in alkali-halide hosts that had been strained by mixing different halide ions.[1]

The implantation study provided the first convincing evidence that the low-energy excitations in the disordered crystalline and in the amorphous phase have the same physical nature, and thus strengthened the conclusion that the glasslike excitations discovered in many chemically disordered crystals are identical to those observed in structurally disordered amorphous solids. This provided further incentive to study the evolution of the glasslike excitations in crystals containing increasing amounts of disorder. In the work to be described here, we will report on the evolution of these states in several alkali-earth fluorides with increasing chemical disorder, and will explore in particular the saturation of the states, and the effect of random stresses. In a separate publication, work on the elastic properties of alkali halides containing substitutional cyanide ions will be reported.[22]

To date, only four systematic studies of disordered crystals as a function of their chemical composition have been undertaken, with limited success. In $(KBr)_{1-x}(KCN)_x$,[9] the most thoroughly studied example, difficulties arose even for dilute compositions, i.e., $x<10^{-4}$, since the isolated CN^- ions themselves have tunneling states that severely influence the elastic and thermal properties of the crystal.[2] In the intermediate range, up to $x\sim 0.10$, the low-energy excitations can still be viewed as the tunneling states of individual CN^- ions, modified however, by elastic interactions that were believed to mask the evolution of the glasslike excitations.[23,24] Only for $x\geqslant 0.25$ do these individual tunneling states appear to become unimportant.[25] At these high concentrations, however, the glasslike lattice vibrations are already fully developed. This problem was avoided in $(NaCl)_{1-x}(NaCN)_x$, in which the tunneling states of the individual CN^- ions have little influence on the thermal and elastic properties of the host, since their tunnel splittings are very small. In this case, however, problems involving solubility prevented a detailed investigation of the intermediate range of compositions, and thus the approach to glasslike lattice vibrations.[26] A similar problem arose in crystalline $B_{1-x}C_x$.[7] In the boron-rich B_9C, glasslike lattice vibrations were observed, and were, in fact, determined to be equal to those observed in structurally amorphous B_9C; however, only one intermediate composition, $B_{13}C_2$, was available, which is not enough to explore the evolution of the low-energy excitations.

The most successful study of the evolution of glasslike lattice vibrations was achieved in $(BaF_2)_{1-x}(LaF_3)_x$.[27] From measurements of the low temperature (>0.1 K) specific heat and thermal conductivity, and of the internal friction above approximately 1 K, it was concluded that low-energy excitations with a constant spectral density occurred already at LaF_3 concentrations as small as $x=0.045$. Their spectral density increased with increasing x, saturating at $x\geqslant 0.33$ and at a value inside the range typical for amorphous solids. The observation of a uniform spectral density occurring in a crystal containing only little chemical disorder ($x\geqslant 0.045$) suggests that the mechanism leading to the uniform spectral density already exists even in crystals with relatively low disorder. This observation will be thoroughly tested in the present investigation by extending the internal friction measurements over a wider range of composition and temperature, and also by including measurements of the speed of sound. It will be carried out on several alkali-earth fluorides containing LaF_3. For $(CaF_2)_{1-x}(LaF_3)_x$ and $(SrF_2)_{1-x}(LaF_3)_x$, it will be shown that a uniform spectral density of the tunneling states does not occur for small x, but only in the most highly disordered crystals. Upon closer inspection, and including previously unpublished measurements below 1.0 K, it will be shown that the same conclusion is also valid for $(BaF_2)_{1-x}(LaF_3)_x$,[27] even with the limited resolution of this earlier work. In the mixed host $[(BaF_2)_{0.5}(SrF_2)_{0.5}]_{1-x}(LaF_3)_x$, on the other hand, a uniform spectral density $\overline{P}$ of the tunneling states exists already for small La concentrations. The consequences of these findings for our understanding of the low-energy excitations in solids will be discussed.

II. EXPERIMENT

A. Mixed fluoride crystal samples

The disordered crystals studied here belong to a large class of mixed fluorides of the form $(MF_2)_{1-x}(RF_3)_x$, where M is Ca, Sr, Ba, and R is La, Y, Lu, or any rare earth that forms a 3^+ ion. These mixed crystals are known to maintain the fluorite crystal structure up to dopant concentrations as

TABLE I. Reference values for the crystals investigated. The lattice constants and mass densities are taken from (Ref. 49), the ionic radii from (Ref. 50). The values of $N=4/a^3$ are the number densities of alkaline earth (e.g. Ca^{2+}) sites per unit cell, useful calculating the number of substituted La^{3+} ions, and thus the number of interstitial F_i^- ions per volume.

Crystal	a (Å)	N (cm^{-3})	ρ (g/cm^3)	Crystal ion	Ionic radius (Å)
CaF_2	5.463	2.45×10^{22}	3.18	Ca^{2+}	0.99
SrF_2	5.800	2.05×10^{22}	4.24	Sr^{2+}	1.12
BaF_2	6.200	1.68×10^{22}	4.89	Ba^{2+}	1.34
				La^{3+}	1.06
				F^-	1.33

TABLE II. Collection of data obtained on the fluorides studied. Column (I), composition in the melt; column (II), mole percent LaF_3 as determined in most cases by x-ray fluorescence; column (III), measured mass density; column (IV), lattice constant, determined by x-ray diffraction; column (V), transverse speed of sound measured in torsion at 1.0 K and ≈90 kHz using Eq. (10); column (VI), tunneling strength $C=\bar{P}\gamma^2/\rho v^2$ for transverse sound waves as determined from the measured $\Delta v/v_0$ using Eq. (9), except for the $(CaF_2)_{0.8}(LaF_3)_{0.2}$; column (VII), crossover temperature T_{co} determined from $\Delta v/v_0$ using Eq. (14); column (VIII), coupling energy γ_t determined from T_{co} using Eq. (15); column (IX), spectral density $\bar{P}$ determined from $\Delta v/v_0$ using Eq. (12). The crystals for which both internal friction and speed of sound are described well with the tunneling model are marked with a bullet in column (I). In all other crystals, the tunneling model fits are usually quite good for $\Delta v/v_0$, with the fit parameters and quantities so derived listed in columns (VI)–(IX); these parameters, however, do not fit the internal friction well, as shown in the figures. The values for a-SiO_2 agree closely with previously published ones (Ref. 10) and are given for comparison.

(I) Composition in melt	(II) (%)[a]	(III) ρ (g/cm^3)	(IV) a (Å)	(V) $v_{1\,K}$ (km/s)	(VI) $\bar{P}\gamma^2/\rho v^2$ (10^{-5})	(VII) T_{co} (K)	(VIII) γ_t (eV)	(IX) $\bar{P}$ (10^{44}/(J m^3))
CaF_2		3.18	5.469±0.001					
$(CaF_2)_{0.999}(LaF_3)_{0.001}$	0.1[b]	3.18		3.75	0.4	0.083	1.20	0.05
$(CaF_2)_{0.995}(LaF_3)_{0.005}$	0.5[b]	3.21		3.82	0.9	0.118	0.73	0.31
$(CaF_2)_{0.98}(LaF_3)_{0.02}$	1.9	3.28		3.62	3.7	0.132	0.54	2.1
$(CaF_2)_{0.90}(LaF_3)_{0.10}$	8.5	3.54		3.23	7.5	0.122	0.48	4.7
• $(CaF_2)_{0.85}(LaF_3)_{0.15}$	13	3.73	5.548±0.003	3.46	4.6	0.120	0.60	2.2
$(CaF_2)_{0.80}(LaF_3)_{0.20}$[c]	20[b]	3.99[d]		3.69	6.5[c]			
• $(CaF_2)_{0.70}(LaF_3)_{0.30}$	26	4.21	5.634±0.005	3.11	5.7	0.105	0.59	2.6
$(BaF_2)_{0.99}(LaF_3)_{0.01}$	0.8	5.00		2.31				
$(BaF_2)_{0.90}(LaF_3)_{0.10}$[e]	12	5.10		2.33	12	0.080	0.48	5.6
• $(BaF_2)_{0.70}(LaF_3)_{0.30}$[e]	33	5.38	6.105±0.005	2.37[f]	27[g]			
• $(BaF_2)_{0.55}(LaF_3)_{0.45}$[e]	46	5.55		2.40	27[g]			
$(SrF_2)_{0.99}(LaF_3)_{0.01}$	1[b]	4.32	5.803±0.001	2.93				
$(SrF_2)_{0.95}(LaF_3)_{0.05}$	4.6	4.41		2.82	0.4	0.100	0.51	0.21
$(SrF_2)_{0.85}(LaF_3)_{0.15}$	17	4.67		2.91	1.4	0.090	0.67	0.48
• $(SrF_2)_{0.70}(LaF_3)_{0.30}$	32	4.89		3.41	2.5	0.105	0.90	0.68
$(BaF_2)_{0.495}(SrF_2)_{0.495}(LaF_3)_{0.01}$	1	4.66	5.993±0.001	2.57				
• $(BaF_2)_{0.485}(SrF_2)_{0.485}(LaF_3)_{0.03}$	4	4.67		2.33	2.4	0.110	0.28	3.0
• $(BaF_2)_{0.465}(SrF_2)_{0.465}(LaF_3)_{0.07}$	7	4.72		2.52	4.6	0.110	0.35	4.5
a-SiO_2		2.20		3.73	31	0.080	1.00	3.6

[a]Composition analyzed by x-ray fluorescence with the LaF_3 concentration in mol %.
[b]Composition assumed to be that in the melt.
[c]Data and composition information taken from Ref. 51.
[d]Determined by interpolation.
[e]Data and composition information taken from Refs. 27 and 43.
[f]Determined at 4 K.
[g]From thermal-conductivity measurements found in Ref. 15; C was determined to be 28×10^{-5} in Ref. 16.

high as $x\sim0.5$.[28] The substitution of La^{3+} ions for M^{2+} introduces fluorine interstitials (F_i^-) into the lattice to maintain charge balance, and for less than 1% LaF_3, the excess F_i^- enters the lattice at the cubic interstitial site nearest the dopant (La^{3+}) ions.[29] Higher dopant concentrations are believed to form more complicated clusters of La, F and anion-sublattice vacancies.[29–32] For $(CaF_2)_{1-x}(LaF_3)_x$ especially, where the interstitial F_i^- radius (1.33 Å) is substantially larger than both the Ca^{2+} (0.99 Å) and La^{3+} (1.06 Å) ionic radii, it is easy to imagine that the interstitial defects, as well as the clusters of defects and vacancies, introduce stress into the lattice. Large random stresses are also expected in the mixed fluoride hosts, like $(BaF2)_{0.5}(SrF2)_{0.5}$. Table I summarizes some pertinent data on the fluoride hosts and the dopant.

Our samples were obtained both commercially from Optovac[33] or grown specifically for our needs by Dr. John Campbell of the University of Canterbury, New Zealand. Each crystal was grown from the melt under vacuum in a graphite crucible using the Stockbarger technique. The main impurity in the CaF_2 is Sr^{2+}, about 50 ppm, and a trace of Ba^{2+}; the LaF_3 is 99.9% pure where the impurities are neighboring lanthanides of more than one type.[34]

The composition of the crystals used in the study are listed in Table II, first by composition in the melt, then by LaF_3 composition analyzed via x-ray fluorescence. Mass density was determined with the Archimedes principle by weighing samples in air and in degassed water. The lattice constant for selected samples was measured with x-ray diffraction.

B. Torsional oscillator measurements

The internal friction was measured in torsion at 90 kHz, using a composite oscillator technique described in detail by

Cahill and Van Cleve.[35] The crystal samples were prepared by carefully cutting them into bars with a diamond saw such that the torsion axis is parallel to the crystal growth axis. (This is not along a consistent crystallographic direction from boule to boule; the growth axis is generally 45° from ⟨111⟩,[34] but inconsistencies in our measured torsional speeds of sound indicate that this is not always the case.) After cutting, the samples were sanded to rods of $3\times3\ \mathrm{mm}^2$ cross section, with lengths on the order of 2 cm, depending on their shear speed of sound. The sample and quartz transducer were then formed into a composite torsion bar: The cylindrical transducer was first attached to a thin BeCu pedestal[35] with a drop of approximately 25-mg Stycast 2850FT epoxy. The sample was then epoxied to the other end of the transducer, after epoxying a 0.13-nm-thick indium foil [0.18 mm for the strained mixed $(BaF_2)_{0.5}(SrF_2)_{0.5}$ crystals] between sample and transducer to cushion the difference in thermal contraction between them. The sample length was tuned[36] to be one half of a shear wavelength so that the composite oscillator has a resonance frequency at room temperature within 1% of the measured quartz transducer resonance; this adjustment ensures that the epoxy and indium joint between the quartz and sample has almost zero strain, and therefore contributes minimally to the observed internal friction. The oscillator was driven by a set of electrodes that form a quadrupole configuration around the transducer and that simultaneously drive and detect its motion. All measurements were taken at an angular strain amplitude[37] between 2×10^{-9} and 2×10^{-8} to ensure that the oscillators were driven in a strain-amplitude independent range.

To calculate the internal friction of the sample from the internal friction of the composite oscillator, note that it is composed of the transducer and the sample. The internal friction of the composite oscillator is obtained through a linear combination of the energy lost in the transducer and the energy lost in the sample,

$$Q_{\mathrm{co}}^{-1}=\frac{\Delta W_{\mathrm{co}}}{2\pi W_{\mathrm{co}}}=\frac{\Delta W_{\mathrm{tr}}}{2\pi W_{\mathrm{co}}}+\frac{\Delta W_s}{2\pi W_{\mathrm{co}}}, \tag{1}$$

where ΔW is the energy lost per cycle of vibration, and W_{co} is the total energy stored in the composite oscillator. The subscripts co, tr, and *s* represent the composite oscillator, transducer, and sample, respectively. The energy of each part of the oscillator is proportional to its moment of inertia I around the torsion axis times the angular frequency ω squared, that is,

$$W_{\mathrm{co}}=AI_{\mathrm{co}}\omega^2,$$

$$\Delta W_{\mathrm{tr}}=AQ_{\mathrm{tr}}^{-1}I_{\mathrm{tr}}\omega^2,$$

$$\Delta W_s=AQ_s^{-1}I_s\omega^2, \tag{2}$$

where A is some proportionality factor. Combining Eqs. (1) and (2) gives

$$Q_{\mathrm{co}}^{-1}=\frac{I_{\mathrm{tr}}Q_{\mathrm{tr}}^{-1}+I_sQ_s^{-1}}{I_{\mathrm{tr}}+I_s}. \tag{3}$$

Cahill and Van Cleve showed experimentally that I_{tr} was larger than the calculated moment of inertia I_q of the quartz transducer itself, since the finite thickness of the pedestal and epoxy joints that participate in the motion act to slightly increase the effective transducer length. They found that

$$I_{\mathrm{tr}}=(1+\alpha)I_q, \tag{4}$$

with $\alpha\approx0.06$. Substituting the above expression into Eq. (3) gives

$$Q_{\mathrm{co}}^{-1}=\frac{(1+\alpha)I_qQ_{\mathrm{tr}}^{-1}+I_sQ_s^{-1}}{(1+\alpha)I_q+I_s}. \tag{5}$$

The internal friction Q_{tr}^{-1} of the transducer (consisting of the quartz crystal, pedestal, indium foil, and the epoxy), can be determined experimentally by replacing the sample with a crystal of comparable I_s and vanishingly small Q_s^{-1}, like a pure BaF_2 crystal. In that case, the measured Q_{co}^{-1} is the background internal friction of the technique, which we call Q_b^{-1}, and Eq. (5) can be rewritten as

$$Q_b^{-1}=\frac{(1+\alpha)I_qQ_{\mathrm{tr}}^{-1}}{(1+\alpha)I_q+I_s}. \tag{6}$$

By combining this with Eq. (3), we obtain the following expression for Q_s^{-1}, the internal friction of the sample:

$$Q_s^{-1}=\left[\frac{(1+\alpha)I_q+I_s}{I_s}\right]Q_{\mathrm{co}}^{-1}-\left[\frac{(1+\alpha)I_q+I_s}{I_s}\right]Q_b^{-1}. \tag{7}$$

Only quantities that can be measured or calculated appear on the right-hand side of Eq. (7).

The subtraction of the second term, which is the background, is actually not performed in the presentation of the data here. We simply show the first term of Eq. (7) for the doped samples (or the second term for the undoped samples—called ''background''). If $Q_{\mathrm{co}}^{-1}\gg Q_b^{-1}$, the internal friction shown in the figures is essentially that of the sample. In the cases where Q_{co}^{-1} and Q_b^{-1} become comparable, Q_s^{-1} would have to be determined by performing the difference as indicated in Eq. (7); however, for simplicity of presentation, we leave the graphical comparison between the first term and the second term to the reader.

The temperature dependence of the relative sound velocity is defined as

$$\frac{\Delta v}{v_0}=\frac{v(T)-v_0}{v_0}, \tag{8}$$

where $v(T)$ and v_0 are the speed of sound at temperature T, and reference temperature T_0, respectively. Cahill and Van Cleve derived the temperature dependence of the relative sound velocity of the sample in a similar way to the derivation of the internal friction of the sample; therefore we only quote the result,

$$\left.\frac{\Delta v}{v_0}\right|_s=\left[\frac{(1+\alpha)I_q+I_s}{I_s}\right]\left[\left.\frac{\Delta f}{f_0}\right|_{\mathrm{co}}-\left.\frac{\Delta f}{f_0}\right|_b\right], \tag{9}$$

where the subscripts co and *b* represent the compound oscillator with the sample, and with a pure crystal (i.e., background), respectively. In this work, $\Delta f/f_0|_b$ was found to be

on the order of 10^{-7}, which was always negligible relative to the first term in Eq. (9) and therefore can be ignored in the data presented in the figures.

The absolute transverse speed of sound v_t for the sample at or near 1 K (as given in Table II) is calculated from the resonant frequency f_s of the free sample, which in turn is calculated from the measured resonant frequency of the composite oscillator with the equations

$$v_t=\frac{2f_s l}{\beta} \quad \text{and} \quad f_s \simeq f_{\rm co}\left[(1+\alpha)\frac{I_q}{I_s}\left(1-\frac{f_{\rm tr}}{f_{\rm co}}\right)+1\right], \tag{10}$$

where $f_{\rm co}$ is the measured frequency of the composite oscillator, β equals 0.92 for a bar of square cross section,[38] l is the sample length, and the frequency of the transducer $f_{\rm tr}$ is measured before the sample is mounted.

Measurements below 1.5 K were made in a dilution cryostat, and those from 1.5 K to room temperature in an insertable ^{4}He cryostat.[39] We mention in passing that, in the internal friction measurements of the $x=0.019$ and 0.085 samples of $(CaF_2)_{1-x}(LaF_3)_x$ only, we observed very narrow peaks between 30 and 70 K that changed location in temperature, depending on whether the data were taken with an increasing or decreasing temperature sweep. Although we believe these peaks to be most likely some experimental artifacts, we cannot explain their presence or their apparent hysteresis. (They are too sharp to be Debye peaks, and the frequency of the oscillator through these peaks is smooth and continuous, indicating that they are not caused by cracking of the sample.) They have been removed from the data presented here, but are shown in detail in Ref. 36.

III. TUNNELING MODEL

The low temperature (<5 K) elastic data are analyzed with the phenomenological tunneling model (TM).[4,5,40] This model assumes the existence of a constant spectral density $\overline{P}$ of tunneling states [or two level systems (TLS)], which are coupled to longitudinal and transverse elastic strains in the solid with coupling energies $\gamma_{l,t}$, respectively.

At temperatures below about 5 K, and at the frequencies used in our experiments, the tunneling systems dissipate elastic energy in dielectric solids via one-phonon relaxation. Within this regime, the relaxational processes giving rise to internal friction and changes in speed of sound have simple high and low temperature limits; the crossover between the two types of behavior is indicated by the crossover temperature $T_{\rm co}$, the temperature at which the maximum relaxation rate of the TLS equals the angular frequency of the applied strain oscillations. Internal friction is then given by

$$Q_0^{-1}=\begin{cases}\dfrac{\pi^4}{96}C_{l,t}\left[\dfrac{T}{T_{\rm co}}\right]^3 & \text{for} \quad T\ll T_{\rm co} \\ \dfrac{\pi}{2}C_{l,t} & \text{for} \quad T\gg T_{\rm co},\end{cases} \tag{11}$$

where

$$C_{l,t}=\frac{\overline{P}\gamma_{l,t}^2}{\rho v_{l,t}^2}. \tag{12}$$

We call Q_0^{-1} the ''plateau'' value of internal friction, which is directly proportional to the so-called tunneling strength $C_{l,t}$ (transverse or longitudinal subscript depending on the vibrational mode of measurement). Combining the definition of internal friction Q^{-1} as defined in Eq. (1) with Eq. (12), it follows that

$$2\pi Q^{-1}=\frac{\Delta W}{W}=\pi^2\frac{\overline{P}\gamma_{l,t}^2}{\rho v_{l,t}^2}. \tag{13}$$

Thus, $\overline{P}\gamma_{1,t}^2$ can be interpreted as a measure of the energy lost in one cycle, and $\rho v_{1,t}^2$ as a measure of the total energy stored in the oscillator.

The temperature variation of the speed of sound for dielectric solid is given by the TM to be

$$\frac{\Delta v}{v_0}=\begin{cases}C\ln\dfrac{T}{T_0} & \text{for} \quad T\ll T_{\rm co} \\ -\dfrac{1}{2}C\ln\dfrac{T}{T_0} & \text{for} \quad T\gg T_{\rm co},\end{cases} \tag{14}$$

where Δv and v_0 are defined in Eq. (8). Note that the reference temperature T_0 is not to be confused with the tunneling crossover temperature $T_{\rm co}$. For the sake of clarity, we have dropped here and in the following the l,t subscripts on C and v; all values reported here from our torsional oscillator method are transverse. Between the two temperature extremes i.e., near $T_{\rm co}$, numerical integrations of TM predictions for both Q^{-1} and $\Delta v/v_0$ are required, and the resulting curves contain only two parameters, $T_{\rm co}$ and C. The values of the coupling energy γ_t found in Table II were calculated[10] using the crossover temperature $T_{\rm co}$ given by[40]

$$T_{\rm co}=\left[\frac{2\pi\rho\hbar^4\omega}{8k_B^3\left(\dfrac{\gamma_l^2}{v_l^5}+2\dfrac{\gamma_t^2}{v_t^5}\right)}\right]^{1/3} \tag{15}$$

and the empirical relations[6] $v_l\approx 1.65v_t$ and $\gamma_l^2\approx 2.5\gamma_t^2$. The spectral density $\overline{P}$ values in Table II were then calculated from Eq. (12).

The tunneling model has been tested successfully for many amorphous solids, and often a single set of parameters $T_{\rm co}$ and C has been found to fit both internal friction and speed of sound measurements,[6] although some discrepancies have been noted.[6,10,41,42] Here, we show only two examples of discrepancies we need to consider in the evaluation of our data. Figure 1 contains speed of sound and internal friction measured in the present investigation on a rod of a-SiO_2 (Suprasil W) at a frequency of 90 kHz. The solid curve in Fig. 1(a) is a best fit of the speed of sound data to the tunneling model from which the tunneling strength C and the crossover temperature $T_{\rm co}$ are determined, and listed in Table II. Note that above the maximum, the measured $\Delta v/v_0$ decreases more rapidly than predicted by the model; this is one of the frequently observed discrepancies. The second discrepancy is shown in Fig. 1(b), where the solid curve is calculated from C and $T_{\rm co}$ as determined in Fig. 1(a). It agrees quite well with the data, although a perfect fit would require a small change of C and $T_{\rm co}$. In order to achieve the best fits to both sets of elastic data, some averages of C and

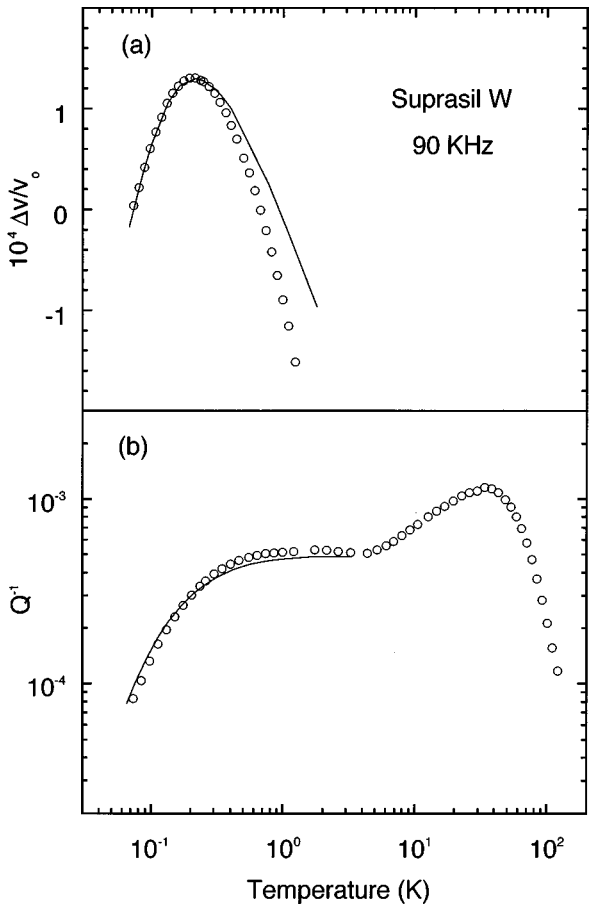

FIG. 1. Vitreous silica (Suprasil W, OH^- concentration <5 ppm), measured in torsion at 90 kHz on a cylindrical rod 4 mm in diameter. (a) Relative variation of the transverse speed of sound at low temperatures, with v_0 the velocity at the lowest temperature of measurement, and (b) internal friction below 100 K. The solid curve in (a) is a fit to the tunneling model near the temperature of the velocity maximum and below, as described in the text. The tunneling strength $C=3.1\times10^{-4}$ and the crossover temperature $T_{co}=80$ mK determined from this fit are listed in Table II. The same parameters also fit the internal friction quite well, illustrating the applicability of the tunneling model to this amorphous solid. An almost perfect fit to the internal friction (not shown) would be achieved by using $C=3.6\times10^{-4}$, and $T_{co}=95$ mK. For a recent discussion of the internal-friction peak at 35 K, which is associated with thermally activated relaxation, see Rau *et al.* (Ref. 52).

T_{co} have previously been used that fit both sets more equally (e.g., Refs. 6 and 16). Alternatively, C has been determined from the internal friction in the plateau, and T_{co} from the speed of sound near the maximum.[10] Since the speed-of-sound data measured in this investigation generally resemble the TM prediction qualitatively better than the internal-friction data, as will be seen in the following, we will use the method indicated in Fig. 1, i.e., we will determine both C and T_{co} from the speed of sound at temperatures at and below the velocity maximum, and then test the agreement between predicted and measured internal friction.

IV. EXPERIMENTAL RESULTS

In $(CaF_2)_{1-x}(LaF_3)_x$, Fig. 2 shows that even for small x

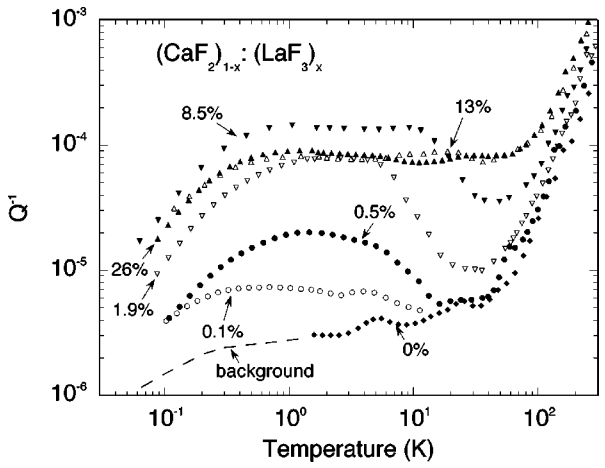

FIG. 2. Internal friction of pure CaF_2 and of $(CaF_2)_{1-x}(LaF_3)_x$ samples for six different concentrations, measured in torsion near 90 kHz. The data points labeled ''0%'' are measurements of the background of the technique using a pure CaF_2 crystal as the sample while the dashed line labeled ''background'' was measured with a quartz crystal in its place. As described in the text and Eq. (7), the internal friction of the samples is determined by taking the difference between the data points and the background. Notice how a broad, temperature-independent internal-friction plateau is observed only for the two largest values of x.

a noticeable increase of the internal friction is observed, although not a temperature-independent plateau. At $x=0.005$, Q^{-1} peaks at $T\approx2.0$ K. As x increases to 0.019 and 0.085, this peak broadens, although it still shows a pronounced drop above approximately 10 K. As x increases to 0.13 and 0.26,

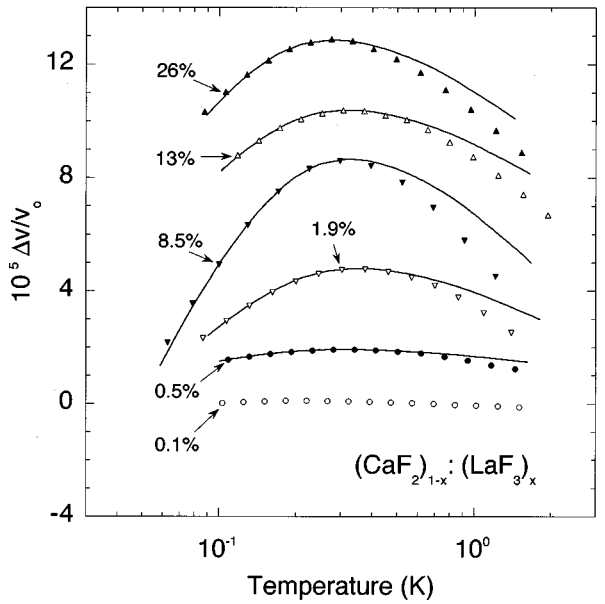

FIG. 3. Relative change in transverse speed of sound for $(CaF_2)_{1-x}(LaF_3)_x$ for the samples shown in Fig. 2 with v_0 the velocity at the lowest temperature of measurement. The data have been shifted vertically to increase the clarity of the presentation. The solid curves are best fits to the tunneling model from near the velocity maximum to low temperatures. The values of the tunneling strength C and the crossover temperatures T_{co} derived from these fits are listed in Table II.

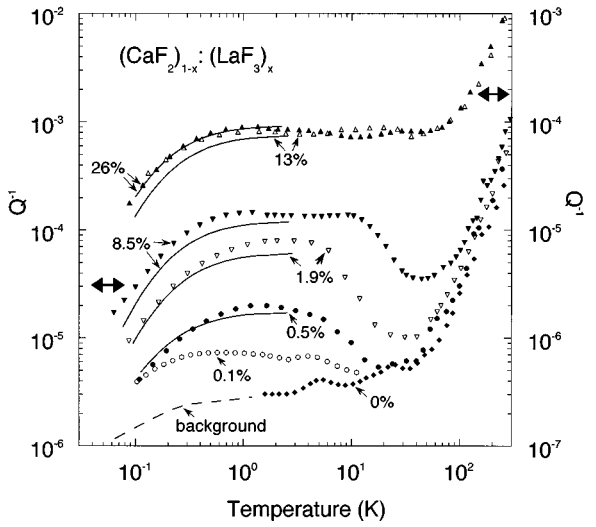

FIG. 4. Same experimental data as in Fig. 2. Note that for the curves for $x=0.13$ and 0.26, the scale on the right is to be used. For all the other curves, use the left scale. The solid curves are calculated using tunneling strengths C and crossover temperatures T_{co} as determined in Fig. 3 (see also Table II). Note that the quality of the fits improves with increasing La concentration x.

this dip vanishes, and only a broad, temperature-independent plateau, indicative of a uniform spectral density of states, is observed between 1 and 20 K. Figure 3 shows the temperature dependent speed of sound for the same samples. The solid curves are best fits to the data from the temperature of the velocity maximum on down using the tunneling model, as described in the previous section; the fits show the same shortcoming as observed in amorphous solids, in that the predicted curve above the velocity maximum exceeds the measured velocities. However, when the values of the tunneling strength C and the crossover temperature T_{co} derived from these fits (listed in Table II) are used to predict the internal friction, a more remarkable disparity is noticed, see Fig. 4. Only for the largest La concentration, $x=0.26$, is the fit considered good; not only in terms of temperature dependence but also in magnitude. The quality of the fit deteriorates for smaller x. Note that as the width of the internal-friction plateau decreases, so does the agreement between predicted and measured magnitude of the internal friction. Thus, these measurements show that although even for the smallest x low-temperature relaxation is observed, the tunneling model, which is based on the assumption of a constant $\overline{P}$, becomes valid only for the most highly disordered crystals.

Thermal conductivity measurements are summarized in Fig. 5 on $(CaF_2)_{1-x}(LaF_3)_x$. For $x=0.20$, they show excellent agreement with the temperature dependence observed in amorphous solids and in agreement with the tunneling model. (The tunneling strength C derived from these measurements is also listed in Table 3 of Ref. 16.) For $x=0.40$, the thermal conductivity above approximately 20 K agrees closely with $x=0.20$, indicating a saturation of the scattering of thermal phonons. These measurements were not extended to lower temperatures, since the sample contained cloudy precipitates expected to lead to additional phonon scattering in that temperature range.

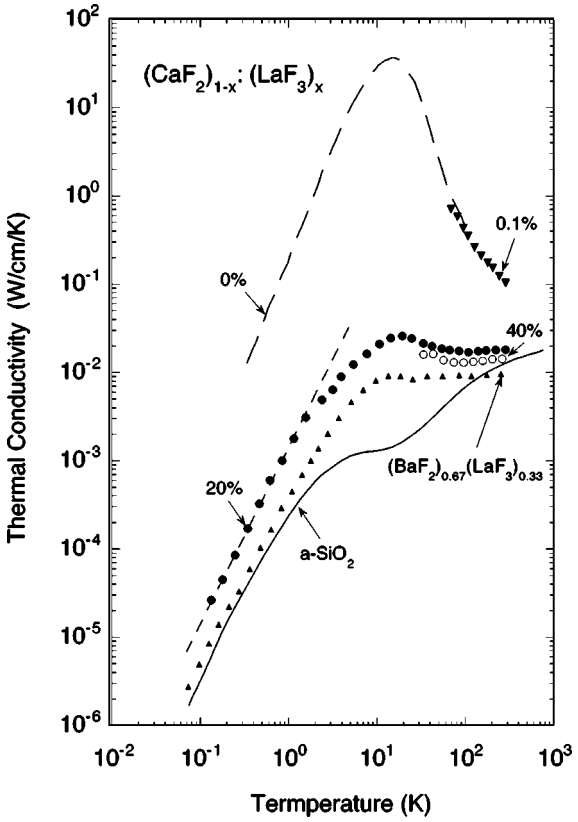

FIG. 5. Thermal conductivity of $(CaF_2)_{1-x}(LaF_3)_x$ for $x=0$ (Ref. 53), $x=0.001$ (Ref. 43), $x=0.20$ (Refs. 43 and 51), $x=0.40$ (Ref. 43), and $(BaF_2)_{0.67}(LaF_3)_{0.33}$ (Ref. 15). The thermal conductivities of $(BaF_2)_{0.67}(LaF_3)_{0.33}$ (Ref. 15) and of a-SiO_2 (Refs. 54 and 55) are shown for comparison. The dashed line through the $x=0.20$ data has a value of $1.4\times10^{-3}T^2\,\mathrm{W\,cm^{-1}\,K^{-3}}$ (Ref. 16).

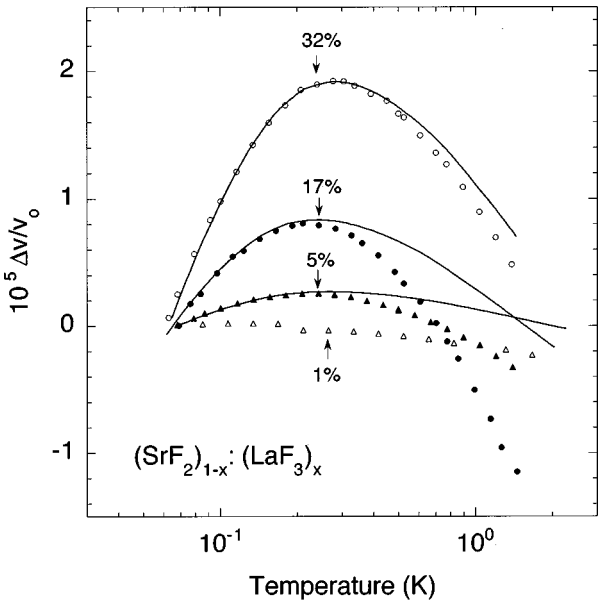

FIG. 6. Relative change of the transverse speed of sound for $(SrF_2)_{1-x}(LaF_3)_x$ for different compositions. The solid curves are best fits of the tunneling model near and below the temperature of the velocity maximum. Tunneling strengths C and crossover temperatures T_{co} are listed in Table II.

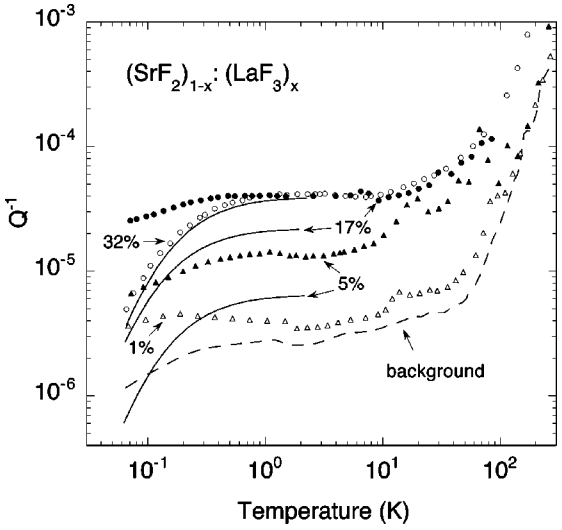

FIG. 7. Internal friction of the same samples shown in Fig. 6. The solid curves are TM fits using the parameters C and T_{co} as determined in Fig. 6. Note that a good fit to the data is obtained only for $x=0.32$. The background was measured with a quartz crystal at the lowest temperatures, then with a pure BaF_2 crystal above 1.5 K. The internal friction of the samples is determined by taking the difference between the data points and the background as described in the text and Eq. (7).

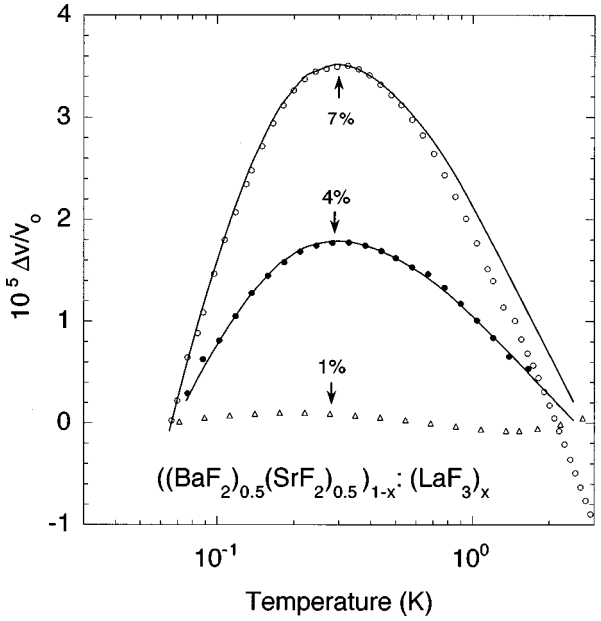

FIG. 8. Relative change of the transverse speed of sound in $[(BaF_2)_{0.5}(SrF_2)_{0.5}]_{1-x}(LaF_3)_x$ for $x=0.01$, 0.04, and 0.07, with v_0 the velocity at the lowest temperatures. The solid curves are best fits of the TM near and below the temperature of the velocity maximum, with the tunneling strength C and crossover temperatures T_{co} listed in Table II.

In $(SrF_2)_{1-x}(LaF_3)_x$, the disparity between the measurements and the prediction of the tunneling model for small x is even more pronounced. Again, the temperature variation of the speed of sound, shown in Fig. 6, seems close to that observed in amorphous solids [see Fig. 1(a)]. However, for $x=0.01$, the internal friction (Fig. 7) peaks around 0.2 K and although a plateau is present for $x=0.17$ and arguably also for $x=0.05$, their magnitudes disagree with the prediction based on the measured speed of sound. Furthermore, the rapid decrease expected for an amorphous solid at the lowest temperatures is missing in both curves. For $x=0.32$, however, the internal friction is very similar to that of amorphous solids, and agrees even quantitatively with the tunneling model prediction using the parameters derived from the speed of sound measurements. Again, the values of C and T_{co} are listed in Table II.

For the mixed host $(BaF_2)_{0.5}(SrF_2)_{0.5}$, the addition of small LaF_3 concentrations also leads to the temperature-dependent speed of sound characteristic for amorphous solids, at least for concentrations exceeding 1%. (See Fig. 8.) The remarkable difference to the CaF_2 and SrF_2 hosts, however, is that the internal friction even for the small concentration $x=0.04$ already shows the temperature dependence characteristic for glasses (Fig. 9). Furthermore, its magnitude agrees perfectly with the prediction based on the values of C and T_{co} determined from the speed of sound in accordance with the tunneling model (listed in Table II), which is shown by the solid curves in this figure. Also, the data for $x=0.04$ and $x=0.07$ appear to scale with concentration. This, however, is not the case for $x=0.01$. The dotted curve in Fig. 9 shows the internal friction calculated on the basis of the higher concentrations, assuming that the internal friction would scale. It is clearly much higher than the measured internal friction for $x=0.01$. (Note that the effect of the defects is only the difference between the measured data and the background. The latter, however, is not known with certainty in this case.)

The measurements on the CaF_2 and SrF_2 hosts have shown that low-energy excitations well described by the tunneling model—which requires a constant spectral density $\overline{P}$—occur only at large LaF_3 concentrations. While this seems to contradict the conclusions drawn earlier for the

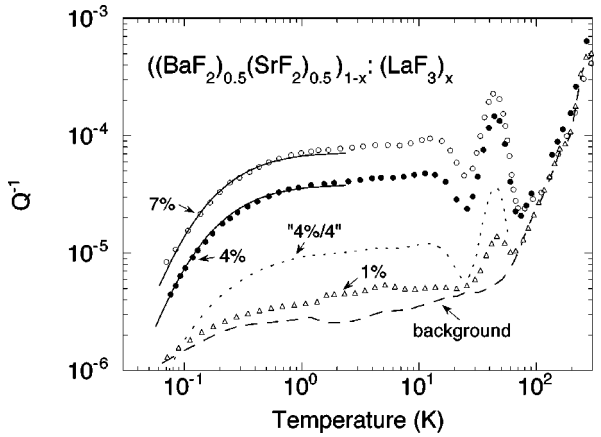

FIG. 9. Internal friction of $[(BaF_2)_{0.5}(SrF_2)_{0.5}]_{1-x}(LaF_3)_x$ for the same samples shown in Fig. 8. The internal friction of the samples is determined by taking the difference between the data points and the background as described in the text and Eq. (7). Solid curves are calculated with the tunneling model using the parameters determined from the speed-of-sound measurements (Fig. 8, see also Table II). Note the excellent agreement for the two higher LaF_3 concentrations. The short-dashed curve labeled ''4%/4'' is the value of the 4% data divided by 4, which lies clearly above the measured data for 1% LaF_3.

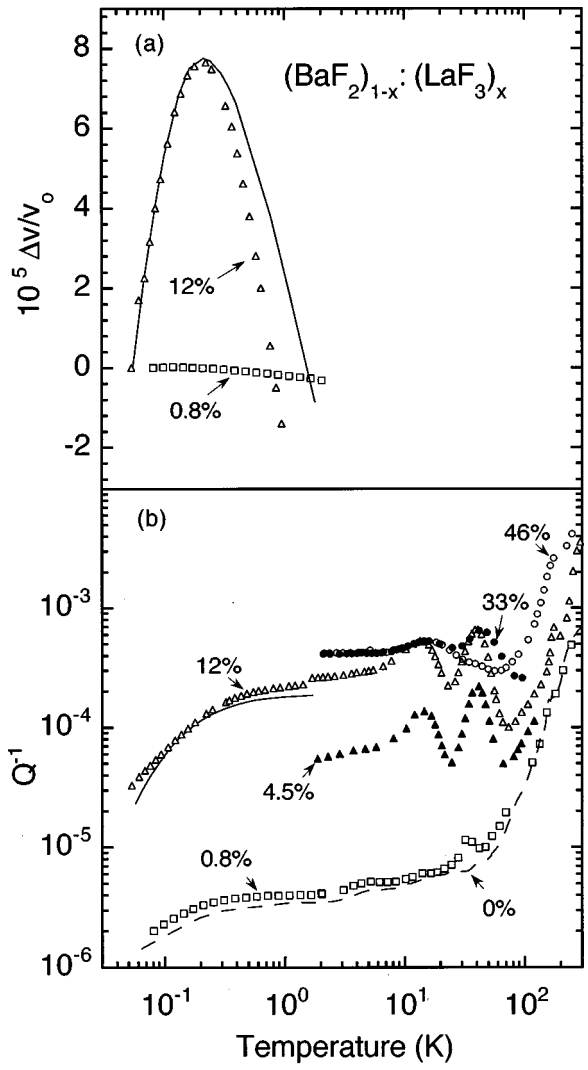

FIG. 10. $(BaF_2)_{1-x}(LaF_3)_x$. (a) Relative variation of the transverse speed of sound, with v_0 the velocity at the lowest temperatures (Table II). The solid curve is the best fit to the data near and below the velocity maximum. The resulting parameters C and T_{co} are listed in Table II. For the smaller concentration, no maximum can be discerned. (b) The data for the temperature region >1.0 K are from Ref. 27 and for the temperature region <1.0 K are from Ref. 43. The solid curve is calculated using the parameters C and T_{co} determined from the sound velocity (listed in Table II). The data for the 0.8% sample below 2.0 K were obtained in this investigation on another sample and agreed perfectly with the previously reported results in the temperature range of overlap. The dashed line is the background as defined in Eq. (6) and shown in Fig. 7.

BaF_2 host, a closer look at the latter data shows that for this host as well, good tunneling model behavior is evidenced only for the large LaF_3 concentrations. In Fig. 10(a), we show previously unpublished data by Cahill of the temperature dependence of the speed of sound for $x=0.12$.[43] As with the fluoride hosts studied here, these results closely resemble those observed in amorphous solids [Fig. 1(a)]. However, the internal friction predicted by the tunneling model on the basis of these measurements agrees only relatively poorly with the measurements shown in Fig. 10(b). Also note that a truly temperature-independent internal friction appears to occur only at even larger values of x ($x=0.33$ and 0.46). We also refer to the measurements of the thermal conductivity shown in Fig. 2 (b) of Ref. 27: For $x=0.045$, its temperature dependence does not seem to follow a power law indicative of a uniform spectral density of tunneling states, in contrast to the power law found for the larger LaF_3 concentrations, or for amorphous solids. The slight, yet distinct curvature observed instead for $x=0.045$ may be another indication for the nonuniform spectral density. While neither of these observations by themselves can be considered as conclusive, together with the results obtained here for the CaF_2 and SrF_2 hosts they provide sufficiently strong evidence to support our conclusion that a behavior consistent with the tunneling model is observed also in the BaF_2 host only in the limit of large LaF_3 concentrations. In the mixed host $(BaF_2)_{0.5}(SrF_2)_{0.5}$, however, a uniform $\overline{P}$ is observed for small LaF_3 concentrations. Its magnitude increases with increasing x, although the effect for $x=0.01$ appears to be small.

The internal-friction data in the BaF_2 host for $x=0.008$ below 2.0 K were obtained in the present investigation on a different sample than the one measured by Cahill and Pohl.[27] They agree perfectly with the earlier data in the temperature range of overlap and illustrate the reproducibility of the measurements. Note also the almost negligible effect this La concentration has on the internal friction of the BaF_2, in contrast to CaF_2 where even 0.1% has a noticeable effect.

The characteristic and most mysterious feature of structurally amorphous solids is not so much the uniform spectral density of the tunneling states, $\overline{P}=\text{const}$, but that the tunneling strength C lies in a narrow region, as mentioned in the Introduction. In the three fluoride hosts BaF_2, CaF_2, and SrF_2, the tunneling strength C in the limit of large LaF_3 concentrations appears to saturate in, or at least close to the glassy range, at 2.7×10^{-4}, 5.7×10^{-5}, and 2.5×10^{-5}, respectively, see Table II, while for the mixed host $(BaF_2)_{0.5}(SrF_2)_{0.5}$, saturation has not been reached yet at a value of $C=4.6\times10^{-5}$ for 7% LaF_3.

V. DISCUSSION

Before discussing these data, let us remember the evolution of low-energy excitations in ion-implanted crystal silicon reported by Liu *et al.*[19] There, it had been concluded that the primary origin of the low-energy excitations was a disorder occurring in the crystalline phase that also persisted in the amorphous phase. It is well known that ion implantation leads to vacancies and interstitials, and aggregate centers. It had been suggested that these centers have low-energy excitations connected with some slight structural rearrangement, and their spectral distribution will be broadened by the random stresses caused by all the defect centers in the crystal. As their number density increases with implantation dose, the stresses will increase, until locally the yield stress has been reached, and the lattice rearranges. This leads to a saturation of the defects with the low-energy excitations, and this saturated density persists as the dose increases by two more orders of magnitude, and exists even in the amorphous phase. This picture emphasizes the local yield stress, and we therefore want to note an empirical, qualitative connection between this quantity and the low-energy excitations. For the

majority of the amorphous solids, the tunneling strength C falls into the glassy range.[7]

$$10^{-4} < C < 10^{-3}. \tag{16}$$

Using an average value of $C = 3 \times 10^{-4}$, Eq. (12) can be rewritten as

$$\frac{\overline{P}\gamma^2}{\rho v^2} \approx 3 \times 10^{-4}. \tag{17}$$

For transverse sound in crystals with cubic symmetry and amorphous solids, ρv^2 is the shear modulus G. For the amorphous solids as compiled by Medwick, White, and Pohl,[7] G varies by a factor of 70 [between the polymer polyethylteraphthalate and amorphous boron]. Hence, the near universality of C for most glasses means that $\overline{P}\gamma^2$ is proportional to the shear modulus. Yield stress and shear modulus are related for nearly perfect crystals although in the disordered crystals, a similar relationship does not exist.[44] It does, however, not seem unreasonable to assume that the local yield stress that governs the motion on the atomic scale, may increase with increasing shear modulus even in chemically or structurally disordered solids. With this assumption, the universality expressed in Eq. (17) can be interpreted as indicating a relation between $\overline{P}\gamma_{l,t}^2$ and the local yield stress. The absence of tunneling states in the hydrogenated a-Si can be interpreted with the picture that the hydrogen somehow eliminates the random stresses that are generally inherent in the amorphous structure and that are needed for the creation of the TLS.

In the present data, the low-temperature elastic measurements of the pure (i.e., not the mixed) fluoride hosts with small La dopings show a striking dissimilarity between the different hosts. In CaF_2, 0.1% LaF_3 has a noticeable effect on the internal friction, Fig. 4, although its temperature dependence clearly does not resemble that predicted by the tunneling model. In the SrF_2 host, the effect is qualitatively similar, although considerably weaker. In BaF_2, the effect of 0.8% LaF_3 is even smaller. Yet despite these differences, a constant $\overline{P}$ develops for large LaF_3 concentrations, say $x = 0.20$ or larger, for all three hosts; and simultaneously the tunneling strengths saturate at values in, or close to, the glassy range. Following the interpretation offered for the saturation in the ion-implanted Si, we postulate that the random stresses at these concentrations have reached a sufficient level so that the local yield stress is attained, leading to the saturation of C at or near the glassy range. The alternative explanation in which a saturation is reached because of quadrupolar interactions between a random array of defects—as first suggested by Klein and co-workers.[45,46] and explored in detail by Sethna and Chow[47] for $(KBr)_{1-x}(KCN)_x$, and recently reviewed by Parshin for amorphous solids[48]—cannot be excluded, since not enough is known about the defects in our case. However, the picture of a large concentration of interacting elastic quadrupoles, which have to be expected to be different in the different crystals containing glasslike excitations, as well as in the amorphous solids, appears to us as somewhat artificial.

In the mixed Ba-Sr fluoride host, a constant $\overline{P}$ already occurs at small LaF_3 concentrations. We take this as evidence for the crucial role played by random stresses in this case; they are large enough to spread out the tunneling states, at least once a particular threshold has been exceeded ($x = 0.01$). Conceivably, this threshold is related to the fact that in both the SrF_2 and the BaF_2 hosts, the defects in this concentration range also show very little relaxational damping because they are structurally simple (e.g., interstitial F^- ions and substitutional La^- ions), and therefore immobile. Hence, random stresses have no effect either. At higher concentrations, more complex centers form, which are susceptible to random stresses. In the mixed host, the random stresses are not large enough to exceed the yield stress. In that case, saturation of the tunneling strength would require a larger LaF_3 concentration in this mixed host. Larger random stresses leading to saturation without large LaF_3 concentrations can perhaps be expected in mixed Ca-Ba fluoride host crystals, because of the larger mismatch in the ionic radii, see Table I. Unfortunately, such mixed crystals were not available for the present investigation.

VI. CONCLUSIONS

Doping of CaF_2, SrF_2, and BaF_2 with LaF_3 at concentrations of mol % or less leads to very different effects on the elastic properties of the different hosts. At concentrations above 20%, however, glasslike lattice vibrations evolve with a constant spectral density, and their tunneling strength saturates at or near the glassy range. In the mixed Ba-Sr fluoride host, a constant spectral density is observed already at 4 mol %, which demonstrates the importance of random stresses for the evolution of these vibrations. This behavior closely resembles earlier observations of CN^- doped alkali halides: At low concentrations, their low-energy motional states depend on the host [e.g., KBr vs NaCl Ref. 26] but at high concentrations glasslike lattice vibrations evolve in either host,[16] and random stresses in KCl:KBr mixed hosts speed up this evolution.[1] These observations, in conjunction with those on the ion-implanted silicon, demonstrate that the physical nature of the defects is relatively unimportant as far as the evolution of the glasslike excitations is concerned, in particular in terms of their saturation. These studies also emphasize the important role played by random stresses in disordered solids.

ACKNOWLEDGMENTS

It is a pleasure to thank J. A. Campbell for supplying many of the samples used in this investigation. We also thank D. G. Cahill, R. S. Crandall, C. Enss, and Xiao Liu for many illuminating discussions. We are grateful to Emil Lobkovsky and John Hunt of the the Cornell Center for Materials Research for x-ray diffraction and x-ray fluorescence analyses. The Bioacoustics Research Lab at the University of Illinois, Urbana, provided financial support of K.A.T. while this paper was completed. This work was supported by NSF Grant No. DMR-9701972 and by the U.S. Department of Education, Graduate Fellowship Program in Materials Science, Grant No. P200A10148. Additional support was received from the Cornell Center for Materials Research through the use of its Central Facilities.

*Present address: Bioacoustics Research Laboratory, University of Illinois at Urbana-Champaign, IL 61801.
[1] S. K. Watson, Phys. Rev. Lett. **75**, 1965 (1995).
[2] V. Narayanamurti and R. O. Pohl, Rev. Mod. Phys. **42**, 201 (1970).
[3] *Amorphous Solids, Low Temperature Properties*, edited by W. A. Phillips (Springer, Berlin, 1981).
[4] P. W. Anderson, B. I. Halperin, and C. M. Varma, Philos. Mag. **25**, 1 (1972).
[5] W. A. Phillips, J. Low Temp. Phys. **7**, 351 (1972).
[6] J. F. Berret and M. Meissner, Z. Phys. B **70**, 65 (1988).
[7] P. A. Medwick, B. E. White, Jr., and R. O. Pohl, J. Alloys Compd. **270**, 1 (1998).
[8] X. Liu and R. O. Pohl, Phys. Rev. B **58**, 9067 (1998).
[9] J. J. De Yoreo, J. M. Rowe, J. J. Rush, and S. Susman, Phys. Rev. Lett. **51**, 1050 (1983).
[10] J. E. Van Cleve, A. K. Raychaudhuri, and R. O. Pohl, Z. Phys. B **93**, 479 (1994).
[11] F. J. Walker and A. C. Anderson, Phys. Rev. B **29**, 5881 (1984).
[12] P. A. Medwick, R. O. Pohl, and T. Tanaka, Jpn. J. Appl. Phys., Part 1 **10**, 106 (1994).
[13] D. A. Ackerman, D. Moy, R. C. Potter, and A. C. Anderson, Phys. Rev. B **23**, 3886 (1981).
[14] J. J. De Yoreo, R. O. Pohl, and G. Burns, Phys. Rev. B **32**, 5780 (1985).
[15] D. G. Cahill, S. K. Watson, and R. O. Pohl, Phys. Rev. B **46**, 6131 (1992).
[16] K. A. Topp and D. G. Cahill, Z. Phys. B **101**, 235 (1996).
[17] A. K. Raychaudhuri and R. O. Pohl, Phys. Rev. B **46**, 10 657 (1992).
[18] X. Liu, B. E. White, Jr., R. O. Pohl, E. Iwanizcko, K. M. Mahan, B. N. Nelson, R. S. Crandall, and S. Veprek, Phys. Rev. Lett. **78**, 4418 (1997).
[19] X. Liu, P. O. Vu, R. O. Pohl, F. Schiettekatte, and S. Roorda, Phys. Rev. Lett. **81**, 3171 (1998).
[20] R. J. Schreutelkamp, J. S. Custer, J. R. Liefting, W. X. Lu, and F. W. Saris, Mater. Sci. Rep. **6**, 275 (1991).
[21] T. E. Seidel and L. A. Larson, MRS Bull. **17**, 34 (1992).
[22] K. A. Topp and R. O. Pohl (unpublished).
[23] W. Knaak and M. Meissner, in *Disordered Systems and New Materials*, edited by M. Borissov *et al.* (World Scientific, Singapore, 1988), p. 399.
[24] C. Enss, H. Schwoerer, D. Arndt, and M. V. Schickfus, Phys. Rev. B **51**, 811 (1995).
[25] J. J. De Yoreo, W. Knaak, M. Meissner, and R. O. Pohl, Phys. Rev. B **34**, 8828 (1986).
[26] S. K. Watson and R. O. Pohl, Phys. Rev. B **51**, 8086 (1995).
[27] D. G. Cahill and R. O. Pohl, Phys. Rev. B **39**, 10 477 (1989).
[28] R. H. Nafziger and N. Riazance, J. Am. Ceram. Soc. **55**, 130 (1972).
[29] C. R. A. Catlow, A. V. Chadwick, and J. Corish, J. Solid State Chem. **48**, 65 (1983).
[30] N. H. Andersen, H. N. Clausen, J. K. Kjems, and J. Schoonman, J. Phys. C **19**, 2377 (1986).
[31] C. G. Andeen, J. F. Fontanella, M. C. Wintersgill, R. J. Welchers, R. J. Kimble, Jr., and G. E. Matthews, Jr., J. Phys. C **14**, 3557 (1981).
[32] P. J. Bendall, C. R. A. Catlow, J. Corish, and P. W. M. Jacobs, J. Solid State Chem. **51**, 159 (1984).
[33] Optovac Inc., Brookfield Rd., North Brookfield, MA 01535.
[34] J. A. Campbell (private communication).
[35] D. G. Cahill and J. E. Van Cleve, Rev. Sci. Instrum. **60**, 2706 (1989).
[36] K. A. Topp, Ph.D. thesis, Cornell University, 1997.
[37] X. Liu, E. Thompson, B. E. White, Jr., and R. O. Pohl, Phys. Rev. B **59**, 11 767 (1999).
[38] *Handbook of Engineering Mechanics*, edited by W. Flügge (McGraw-Hill, New York, 1962), Chap. 36.
[39] E. T. Swartz, Rev. Sci. Instrum. **57**, 2848 (1986).
[40] A. K. Raychaudhuri and S. Hunklinger, Z. Phys. B **57**, 113 (1984).
[41] C. Enss and S. Hunklinger, Phys. Rev. Lett. **79**, 2831 (1997).
[42] P. Esquinazi, R. Koenig, and F. Pobell, Z. Phys. B **87**, 305 (1992).
[43] D. G. Cahill, Ph.D. thesis, Cornell University, 1989.
[44] S. P. Baker (private communication).
[45] M. W. Klein, B. Fischer, A. C. Anderson, and P. J. Anthony, Phys. Rev. B **18**, 5887 (1978).
[46] M. P. Solf and M. W. Klein, Phys. Rev. B **49**, 12 703 (1994).
[47] J. P. Sethna and K. S. Chow, Phase Transit. **5**, 317 (1985).
[48] D. A. Parshin, Phys. Solid State **36**, 991 (1994).
[49] *Crystals with the Fluorite Structure*, edited by W. Hayes (Clarendon, Oxford, 1974).
[50] *CRC Handbook of Chemistry and Physics*, 67th ed., edited by R. C. Weast (CRC, Boca Raton, FL, 1986), pp. F-157 and F-167.
[51] D. G. Cahill and R. O. Pohl, in *Modern Perspectives on Thermoelectrics and Related Materials*, edited by D. D. Allred, C. Vining, and G. Slack, MRS Symposia Proceedings No. 234 (Materials Research Society, Pittsburgh, 1991), p. 27.
[52] S. Rau, C. Enss, S. Hunklinger, P. Neu, and A. Wuerger, Phys. Rev. B **52**, 7179 (1995).
[53] J. A. Harrington, Phys. Rev. B **1**, 882 (1970).
[54] A. K. Raychaudhuri and R. O. Pohl, Solid State Commun. **44**, 711 (1982).
[55] D. G. Cahill and R. O. Pohl, Phys. Rev. B **35**, 4067 (1987).